Channel Characterization and Finite-State Markov Channel Modeling for Time-Varying Plasma Sheath Surrounding Hypersonic Vehicles

Guolong He[1, 2, *], Yafeng Zhan[1], Ning Ge[1], Yukui Pei[1], Bin Wu[2], and Yuan Zhao[3]

Abstract—Effects on the communication signals caused by the time-varying plasma sheath surrounding hypersonic vehicles are investigated. Using computational fluid dynamics (CFD) technique, Demetriades's plasma turbulence model and finite-difference time-domain (FDTD) algorithm, amplitude variation and phase fluctuation induced by plasma electron density turbulence are obtained, and their statistical properties are analyzed and characterized. Furthermore, a finite-state Markov channel (FSMC) model is proposed, to represent the dynamical effects on electromagnetic wave propagation through plasma sheath. With high accuracy and greatly reduced complexity, the FMSC model could be very useful to develop novel communication techniques for alleviating the radio blackout problem.

1. INTRODUCTION

There has been one long standing obstacle, known as the "radio blackout" problem, associated with hypersonic flight and atmosphere reentry [1–5]. When a vehicle flying at hypersonic velocity or a spacecraft reentering the Earth's atmosphere, all the communication and telemetry signals are lost or at least severely degraded by the plasma sheath around hypersonic vehicles, which is formed by surrounding dissociated and ionized air molecules due to tremendous heat converted from the vehicle's kinetic energy [1–3]. The radio blackout problem has already attracted much attention from both academia and agencies, especially during the days of the Apollo missions. In 1960s–1970s, many ground researches and inflight experiments had been conducted by NASA and the U.S. Air Force to measure the parameters of the plasma sheath, as well as to test some possible mitigation methods [2–4]. However, formation of the plasma sheath coupled with both chemical and thermodynamic processes are still not well understood, some alleviation techniques remain in the development stages with obvious shortages, which leaves this problem unresolved as before.

There have already been many researches dealing with the plasma sheath and investigating its effects on the communication signals [6–13]. However, most of the previous works consider this problem in a time-invariant case, where severe amplitude attenuation and large phase shift are reported [6–10]. Although these steady-state effects are very important, the time-varying effects are also very crucial for communication failure and this has rarely been studied. In [11], Ohler et al. used a general ray-tracing method to investigate high-speed plasma flow of a stationary plasma thruster. In their work, a pure-sine temporal density variation model is assumed and high-order harmonics are observed in the received signals. Gao et al. used the scattering matrix method (SMM) to investigate the effects of plasma sheath on the GPS navigation signals [12]. However, only the electron density turbulence on the boundary layer is considered and fluctuations in other areas are omitted. Recently, Yang et al. simulated

the propagation of QPSK signals though time-varying plasma and constellation circumvolving of the receiving signals was reported in their work [13]. Unfortunately, the plasma slab assumed to be uniform is not the case for practical reentry plasma sheath.

In this paper, we will focus on the electron density turbulence of plasma sheath and its dynamical effects on electromagnetic wave propagation. Moreover, using the parameters extracted from channel characterization, we will propose a Markovian channel model to represent the dynamical effects on the communications signals. To the best of our knowledge, it's the first time that channel modeling of time-varying plasma sheath is presented. The rest of this paper is organized as follows. Section 2 starts with some brief theoretical analysis of interactions between electromagnetic waves and plasma. In Section 3, the general simulation flowchart and some related numerical techniques are introduced. Section 4 presents the results of channel characterization, while the finite-state Markov channel models are proposed and validated in Section 5. Finally, this paper is summarized in Section 6.

2. THEORETICAL ANALYSIS

Plasma is an electrified gas with its atoms dissociated into positive ions and negative electrons. When electromagnetic wave travels thorough the plasma sheath, the electrons of plasma oscillate around their equilibrium positions under the influence of the electric field. Thus part of the wave's energy is absorbed and reflected, especially when the transmission frequency approximates to the plasma frequency. From the Maxwell's equations, we have the relationships between the electric field $\mathbf{E}$, the magnetic field $\mathbf{H}$ and the polarization current density $\mathbf{J}$ in plasma region as follows,

$$
\begin{aligned}
\nabla \times \mathbf{E} &= -u_0 \frac{\partial \mathbf{H}}{\partial t} \\
\nabla \times \mathbf{H} &= \varepsilon_0 \frac{\partial \mathbf{E}}{\partial t} + \mathbf{J} \\
\frac{\partial \mathbf{J}}{\partial t} + v_p \mathbf{J} &= \varepsilon_0 w_p^2 \mathbf{E}
\end{aligned}
\tag{1}
$$

where v_p is the collision frequency of cold, unmagnetic plasma, and w_p is the plasma frequency and has the following expression [1–4, 7],

$$
w_p = \sqrt{\frac{n_e e^2}{\varepsilon_0 m_e}}
\tag{2}
$$

where n_e is the electron density, e the electron charge, m_e the electron mass, and ε_0 the dielectric constant in free space.

From (1), the relative permittivity of plasma $\varepsilon_r(w)$ can be expressed as follows,

$$
\varepsilon_r(w) = 1 - \frac{w_p^2}{w^2 - jwv_p} = R + j \cdot I
\tag{3}
$$

$$
R = \left(1 - \frac{w_p^2}{w^2 + v_p^2}\right), \qquad I = \frac{v_p}{w} \frac{w_p^2}{w^2 + v_p^2}
$$

From (3), the corresponding wavenumber in plasma k can be derived,

$$
k = k_0 \sqrt{\varepsilon_r(w)} = \beta + j\alpha
\tag{4}
$$

$$
\beta = k_0 \sqrt{\frac{(R^2 + I^2)^{1/2} + R}{2}}, \qquad \alpha = k_0 \sqrt{\frac{(R^2 + I^2)^{1/2} - R}{2}}
$$

where $k_0 = w/c$ is the wavenumber in free space. The amplitude attenuation T and phase shift φ can be estimated as follows,

$$
T = \int \alpha \cdot dx, \qquad \phi = \int \beta \cdot dx
\tag{5}
$$

Since the electron density n_e in (2) varies in time, all the above parameters are time-variant.

3. NUMERICAL SIMULATION

Figure 1 illustrates a general flowchart for investigating the dynamical effects of time-varying plasma sheath. The steady-state plasma sheath was firstly obtained by using computational fluid dynamics (CFD) technique. The timescale for multi-species air flow reaction is on the order of milliseconds, while the timescale for electromagnetic wave propagation through plasma sheath is only on the order of nanoseconds. Hence, to simulate time-varying electron density fluctuation, we can just add some noises with particular power density distribution on the steady-state solution. After that, interactions between electromagnetic waves and plasma are evaluated by using finite-difference time-domain (FDTD) algorithm. All these works will be discussed in detail in the following subsections.
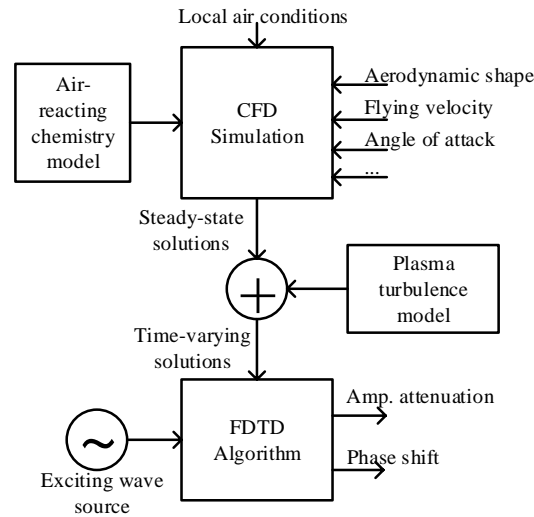
Figure 1. Flowchart for time-varying plasma sheath simulation.

3.1. CFD Simulation for the Steady-State Plasma Sheath

The steady-state distribution of the plasma sheath depends on many factors in reality, such as the vehicle's aerodynamic shape, trajectory, vehicle velocity, angle of attack (AoA), and local air condition. Here, a model of RAM-C blunt body with nose radius of $0.1\,\mathrm{m}$ is established and simulated by using CFD technique. In the simulation, the thermochemical non-equilibrium problem is solved based on Navier-Stokes equations. An eleven-species (N_2, O_2, N, O, NO, N_2^+, O_2^+, N^+, O^+, NO^+, and e) air-reacting chemistry model [14] is employed, and zero degree of AoA is considered. According to the US Standard Atmosphere [15], the static temperature and static pressure are set to $270\,\mathrm{K}$ and $80\,\mathrm{Pa}$, respectively.

Figure 2 illustrates the electron density distribution of the plasma sheath at blunt velocity of $6000\,\mathrm{m/s}$. As can be seen, the air around the vehicle is compressed and a shock wave formed. The plasma electron density in front of the blunt nose region is as high as $10^{20}\,\mathrm{m^{-3}}$. Such a high electron density prevents electromagnetic wave propagation under $30\,\mathrm{GHz}$. Consequently, the onboard antenna is generally mounted in the rear region of the blunt body, which has a significantly lower plasma electron density and much less influence of the plasma sheath.

3.2. The Time-Varying Plasma Turbulence Simulation

A few ground test experiments have investigated the electron density turbulence intensity of plasma sheath [16–20]. Unfortunately, all their data only give qualitative rather than quantitative information. Figure 3 shows the plasma electron density profile radially outward from the onboard antenna at different blunt velocities, which are extracted from the CFD steady-state solutions. For the boundary layer very close to the blunt wall, both the speed and temperature of the air flow dramatically rise from zero
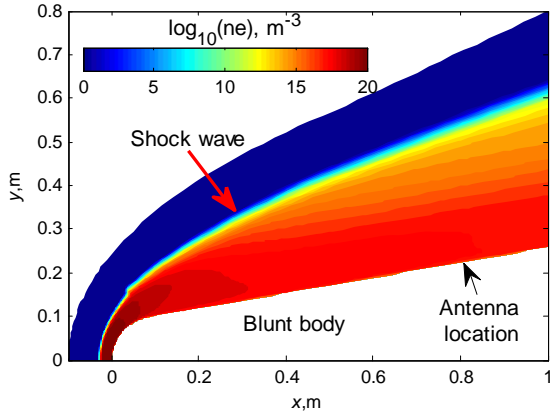
Figure 2. The electron density distribution of the plasma sheath at blunt velocity of 6000 m/s.
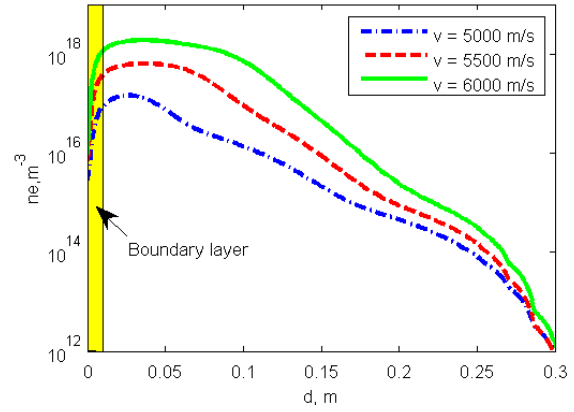
Figure 3. The plasma electron density profile radially outward from the onboard antenna.

to nearly freestream states, thus in this region it has a much stronger turbulence intensity than other areas. According to Demetriades's measurement data obtained from JPL continuous flow hypersonic wind tunnel [18, 19], the power density of such turbulence is pink-colored, the low frequency fluctuation is dominant, while a '$-5/3$' Kolmogorov decay was observed at high frequencies. During our simulation, the relative turbulence intensity for the boundary layer is set to 30% [12, 13, 20]. For the region out of the boundary layer edge, it has a relative lower turbulence intensity. Three scenarios are considered in this paper, i.e., small (5%), medium (10%), and large (15%).

3.3. FDTD Algorithm for Electromagnetic Wave Propagation Analysis

Nowadays, due to its low computational complexity and high efficiency, FDTD algorithm is the most robust and popular method available to investigate electromagnetic wave propagation problems [21, 22]. By applying FDTD algorithm, the Maxwell's equations in (1) are discretized both in space and time, and the electric and magnetic fields are solved and updated in a leap-frog manner. As a time-domain method, FDTD algorithm treats inhomogeneous, nonlinear material properties in a natural way [22]. Moreover, FDTD solutions can cover a wide frequency range just by a single simulation run, which makes it quite useful to investigate the radio blackout problem.

In our work, the stretched-coordinate perfectly matched layer (SC-PML) is employed to truncate the computational boundary, and the media discretization processing for plasma is given in Appendix A [10, 23]. A non-modulated Gaussian pulse with 40 GHz efficient bandwidth is used as the excited incident wave. During each simulation, the transmitted signal through plasma sheath is recorded and compared with the incident signal, thus the wideband characteristic of the plasma sheath can be derived.

4. CHANNEL CHARACTERIZATION

Simulations are carried out over 10000 times for each scenario. Figure 4 illustrates the possible variation regions for different scenarios at blunt velocity of 6000 m/s. The middle line represents the steady-state propagation characteristic without plasma electron density turbulence, while the other six lines are the upper and lower bounds for three scenarios. As can be seen from Figure 4, the amplitude attenuation decreases first then increases with increasing frequency, while the phase shift increases rapidly first and then decreases slowly as the frequency increases. This is because that, the effects near the plasma frequency are the most serious. Hence successful transmission through plasma sheath requires transmission frequencies much higher than the plasma frequency. Figure 5 illustrates the standard deviations of amplitude variation and phase fluctuation caused by the time-varying plasma sheath. For each scenario, the region near 10 GHz has a much larger deviation of amplitude variation than other frequency bands.
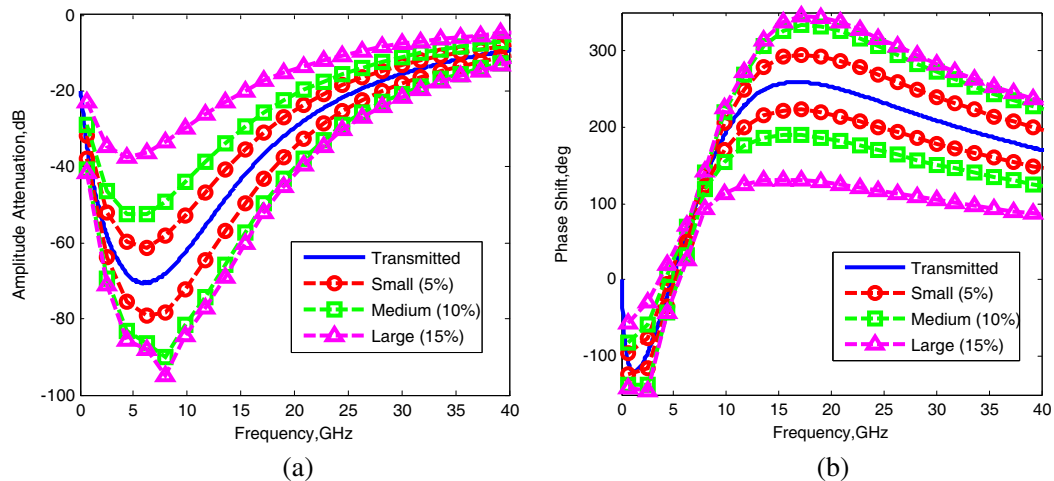
Figure 4. (a) Amplitude attenuation and (b) phase shift caused by the plasma sheath at blunt velocity of 6000 m/s. The middle curves show the steady-state results, while the others show the upper and lower bounds of possible fluctuation under different plasma electron density turbulence intensity.
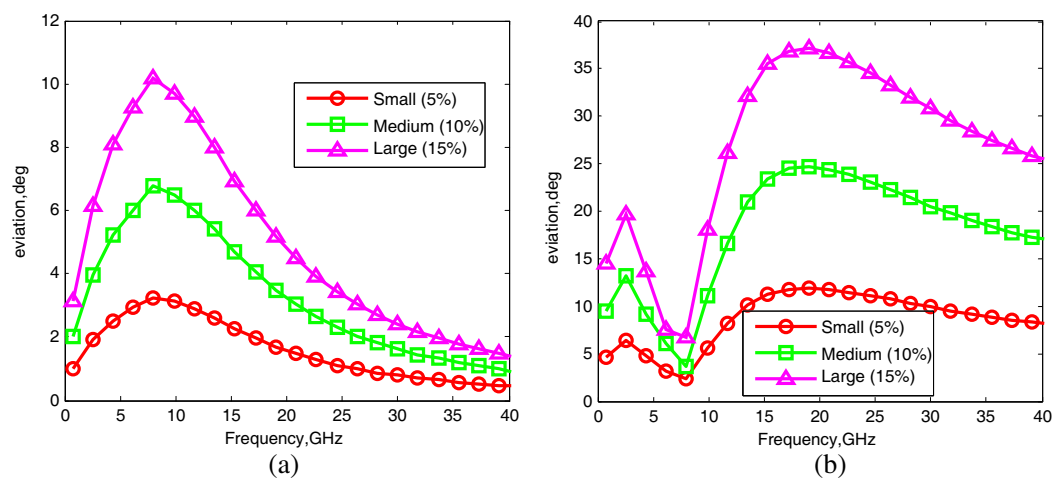

Figure 5. Standard deviations of the effects caused by plasma sheath at blunt velocity of 6000 m/s: (a) amplitude attenuation and (b) phase shift.

Figure 6 illustrates an example of simulated dynamical effects caused by the plasma sheath on Ka-band communication signals, with blunt velocity of 6000 m/s and relative turbulence intensity of 15%. The peak-to-peak values are 12.4 dB for amplitude variation and 171 deg for phase fluctuations, respectively. Table 1 summarizes the statistical properties of these effects at X- and Ka-band. For each velocity, both of the amplitude variation and phase fluctuation increase as the turbulence intensity increases. Compared with X-band, the amplitude variation in Ka-band is relative less, but the phase fluctuation is much larger. This results imply that, high frequency transmission could be considered as a potential method for alleviating the blackout problem, but some other modulation techniques must be investigated rather than the conventional phase-coherent communications.

5. CHANNEL MODELING

Accurate and efficient channel models are of vital importance for developing and evaluating novel communication techniques. Since the effects of the plasma sheath are time-varying, the corresponding channel model must be expressed in terms of statistical averages and probability densities. The finite-
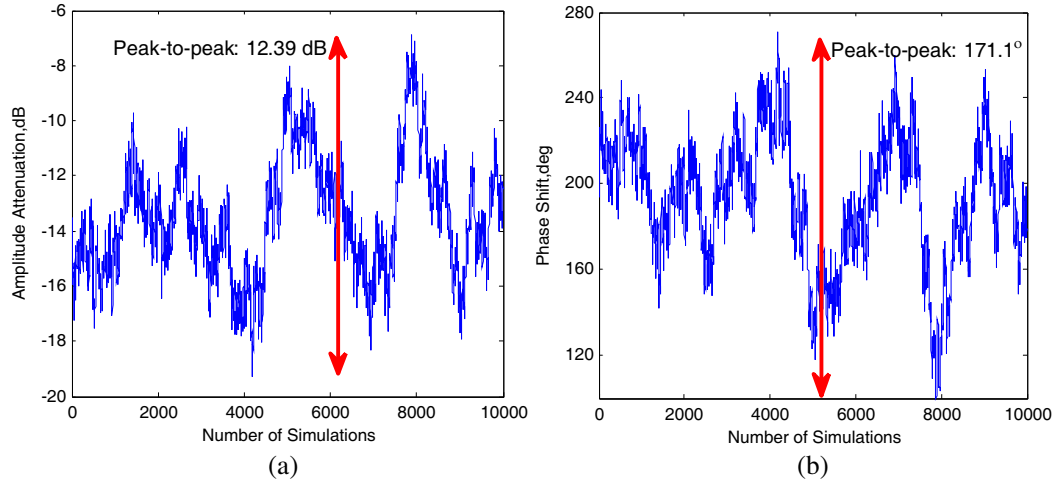
Figure 6. An example of simulated dynamical effects of the plasma sheath on Ka-band communication signals, with blunt velocity of 6000 m/s and relative disturbance intensity of 15%: (a) amplitude attenuation and (b) phase shift.

Table 1. The statistical properties of effects caused by the time-varying plasma sheath.

Blunt velocity (m/s)	Relative turbulence intensity	X-band		Ka-band	
		Amplitude variation (dB)	Phase fluctuation (degree)	Amplitude variation (dB)	Phase fluctuation (degree)
5000	Small (5%)	0.15/0.91*	0.75/4.72	0.02/0.14	0.46/2.83
	Medium (10%)	0.31/1.80	1.55/8.98	0.05/0.28	0.95/5.56
	Large (15%)	0.46/2.67	2.32/13.49	0.07/0.41	1.43/8.31
5500	Small (5%)	0.97/6.00	3.07/19.10	0.16/1.00	2.74/16.89
	Medium (10%)	2.02/11.89	6.33/36.29	0.34/1.98	5.70/33.51
	Large (15%)	3.01/17.38	9.66/56.01	0.50/2.91	8.54/49.56
6000	Small (5%)	3.21/19.82	2.92/19.39	0.70/4.29	9.49/58.55
	Medium (10%)	6.71/40.34	5.08/30.29	1.44/8.54	19.70/116.3
	Large (15%)	10.07/60.38	9.02/61.28	2.14/12.39	29.50/171.1

∗ (Standard derivation/Peak-to-peak value)

state Markov channel (FMSC) model, which was firstly proposed by Gilbert and Elliott at Bell Labs, has attracted quite some attention due to its usefulness to represent such time-varying characteristics [24–27]. In this section, we will partition the power levels of the received signal into a finite number of states and construct the FSMC model of different scenarios, which could enable us to simulate the time-varying effects on electromagnetic wave propagation through plasma sheath with low complexity.

5.1. Parameter Extraction

Based on the statistics of the CFD+FDTD simulated data, first the received signal power levels are assumed to have a Lognormal distribution. In order to determine the parameters of the FMSC model, the data processing and parameter extraction procedures are given as following steps [26, 27],

(1) The lognormal mean u and standard deviation σ values are calculated.

(2) With the range of possible receiving signal power levels, $M+1$ discrete thresholds $\{\Gamma_0, \Gamma_1, \ldots, \Gamma_M\}$ for M states $\{s_1, s_2, \ldots, s_M\}$ are defined, where $\Gamma_0 = 0$ and $\Gamma_M = +\infty$.

(3) Let r denotes the receiving signal power level. According to the pre-defined thresholds, each simulation was assigned to a corresponding state as follows,

$$\text{If } \Gamma_{m-1} < r \leq \Gamma_m, \text{ then state } s_m \text{ is assigned.}$$

(4) The state probability vector π is computed as,

$$\pi(m) = N_m/N;$$

where N_m is the number of simulations in state s_m, and N is the total number of simulations.

(5) The state transition probability matrix P is computed as,

$$p(m, n) = N_{mn}/N_m;$$

where N_{mn} is the number of transitions from state s_m to state s_n.

Here we use the equal probability (EP) approach proposed in [24] to partition the regions of each state, and the number of states are set to 8 as suggested by previous literatures [24–26]. A Ka-band FSMC model with blunt velocity of $6000\,\text{m/s}$ and relative disturbance intensity of 15% is presented as an example in Appendix B.
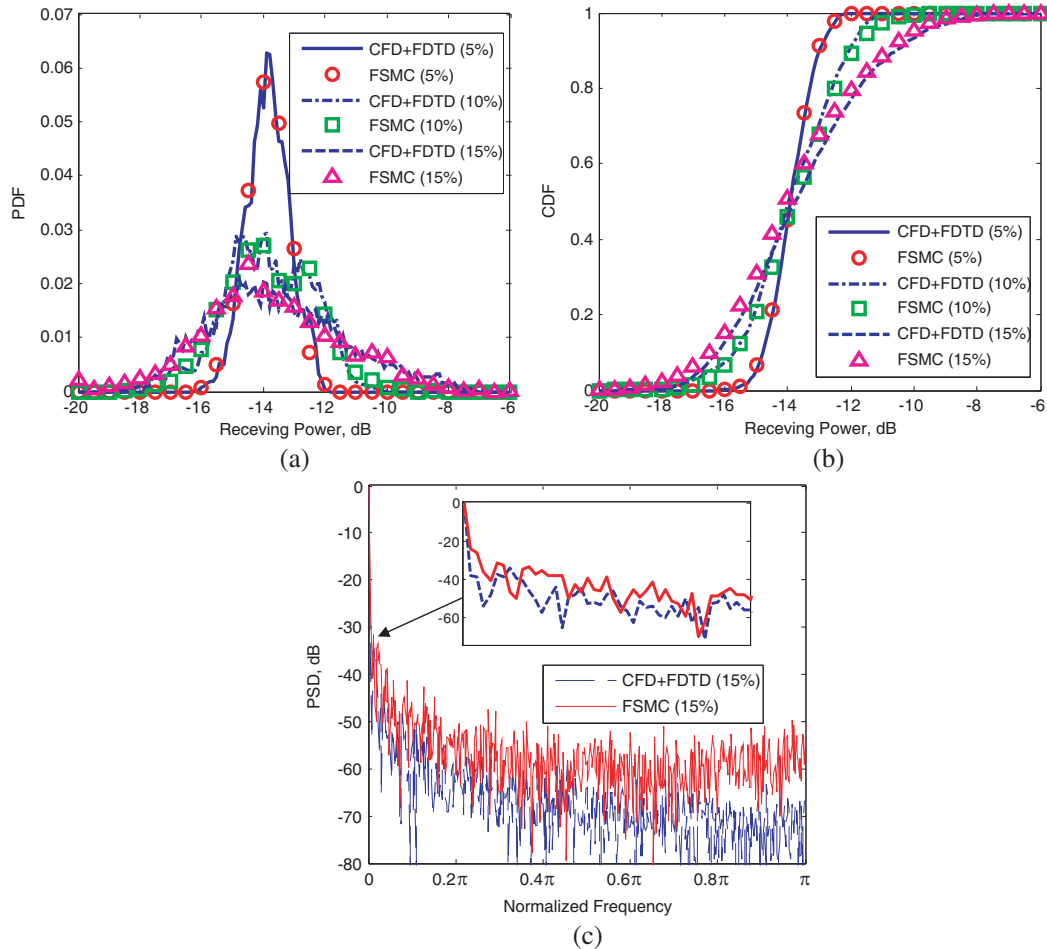

Figure 7. Comparison between results from CFD+FDTD simulation and the FMSC model at Ka-band and blunt velocity of $6000\,\text{m/s}$: (a) PDF, (b) CDF, and (c) PSD.

5.2. Model Validation

Once obtaining the required parameters, a Markovian chain can be generated. In order to verify the effectiveness of the obtained FMSC model, the results will be compared with those from CFD+FDTD simulation. Two primary statistics and one secondary statistic, probability density function (PDF), cumulative distribution function (CDF) and power spectrum density (PSD), are investigated under different scenarios. Figure 7 illustrates the results from CFD+FDTD simulation and the FMSC model at Ka-band and blunt velocity of $6000\,\text{m/s}$. As shown in Figure 7(a), although each scenario has similar mean values near $-14\,\text{dB}$, the deviation increases as the plasma electron density turbulence intensity increases. The PDF of small turbulence intensity is much sharper than the PDF of the other two scenarios. This implies that again, signal fluctuations for large turbulence intensity are much more severe than small turbulence. Comparisons of CFD and PSD are presented in Figures 7(b) and 7(c), excellent agreements are obtained for all three statistics. For other blunt velocities, similar results and good agreements are also observed.

6. CONCLUSION

The radio blackout problem stands as one long difficulty for hypersonic flight and atmosphere reentry. In this paper, the time-varying plasma sheath surrounding hypersonic vehicles and its dynamical effects on the communication signals are investigated. First the CFD technique is used to obtain the steady-state distribution of the plasma sheath, after adding some turbulence on the plasma electron density, interactions between electromagnetic waves and plasma sheath are investigated by using FDTD algorithm. Amplitude variation and phase fluctuation of the communication signals and their statistical properties are analyzed and characterized under different scenarios.

Furthermore, a finite-state Markov channel model is proposed to represent the dynamical effects of plasma sheath on electromagnetic wave propagation. In the FMSC model, the power levels of the received signal are partitioned into a finite number of states, and the time-varying process is modeled as a Markovian chain. Compared to the CFD+FDTD method, the FMSC model has high accuracy and much lower complexity. In future, we would attempt to develop novel communication techniques to reduce the blackout period or alleviate the blackout problem entirely. One possibly feasible approach is that, state transition memories of the FSMC model could be extracted and utilized to improve the performance of the communication system.

APPENDIX A. MEDIA DISCRETIZATION PROCESSING FOR PLASMA

When implementing the FDTD algorithm, the frequency-dependent permittivity of plasma in (3) must be transferred into time domain to get the update equation. The bilinear transform technique is employed in this work [10, 23],

$$jw \rightarrow \frac{2}{\Delta t}\frac{1 - z^{-1}}{1 + z^{-1}} \tag{A1}$$

where a multiplication of z^{-1} in the frequency domain corresponds to a time delay of Δt in discrete-time domain.

Substituting (A1) into (2), the corresponding time-domain update equation for the electrical field $\mathbf{E}$ from the electronic density $\mathbf{D}$ can be derived,

$$\mathbf{E}^{q+1} = b_0\mathbf{D}^{q+1} + b_1\mathbf{D}^q + b_2\mathbf{D}^{q-1} + a_1\mathbf{E}^q + a_2\mathbf{E}^{q-1} \tag{A2}$$

where the superscript q denotes the time series, and the coefficients in (A2) are related to the parameters of plasma,

$$\begin{cases} P = 4 + 2v_p\Delta t + w_p^2\Delta t^2 \\[2mm] a_1 = \dfrac{-8 - 2w_p^2\Delta t^2}{P}, \quad a_2 = \dfrac{4 - 2v_p\Delta t + w_p^2\Delta t^2}{P} \\[2mm] b_0 = \dfrac{4 + 2v_p\Delta t}{\varepsilon_0 P}, \quad b_1 = \dfrac{-8}{\varepsilon_0 P}, \quad b_2 = \dfrac{4 - 2v_p\Delta t}{\varepsilon_0 P} \end{cases} \tag{A3}$$

APPENDIX B. AN EXAMPLE OF THE FSMC MODEL

As an example, the FMSC model at Ka-band with blunt velocity of 6000 m/s and relative disturbance intensity of 15% is presented below. The lognormal mean and standard deviation are $u = -13.5182$ and $\sigma = 2.1412$.

The state transition probability matrix is

$$P = \begin{bmatrix} 0.8949 & 0.1051 & 0 & 0 & 0 & 0 & 0 & 0 \\ 0.0902 & 0.7654 & 0.1443 & 0 & 0 & 0 & 0 & 0 \\ 0 & 0.1425 & 0.7095 & 0.1460 & 0 & 0 & 0 & 0 \\ 0 & 0 & 0.1698 & 0.6592 & 0.1688 & 0 & 0 & 0 \\ 0 & 0 & 0 & 0.1880 & 0.6655 & 0.1447 & 0 & 0 \\ 0 & 0 & 0 & 0 & 0.1434 & 0.7238 & 0.1309 & 0 \\ 0 & 0 & 0 & 0 & 0 & 0.1398 & 0.7828 & 0.0774 \\ 0 & 0 & 0 & 0 & 0 & 0 & 0.0599 & 0.9401 \end{bmatrix}$$

And the state probability vector is

$$\pi = \begin{bmatrix} 0.1237 & 0.1441 & 0.1446 & 0.1226 & 0.1106 & 0.1116 & 0.1059 & 0.1369 \end{bmatrix}$$

From these parameters, a Markovian chain can be generated with specified statistical properties.

ACKNOWLEDGMENT

REFERENCES

1. Rybak, J. P. and R. J. Churchill, "Progress in reentry communications," *IEEE Transactions on Aerospace and Electronic Systems*, Vol. 7, No. 5, 879–894, 1971.

2. Akey, N. D., "Overview of RAM reentry measurements program," *The Entry Plasma Sheath and Its Effects on Space Vehicle Electromagnetic Systems*, 19–31, 1970.

3. Hartunian, R. A., G. E. Stewart, S. D. Fergason, T. J. Curtiss, and R. W. Seibold, "Causes and mitigation of radio frequency (RF) blackout during reentry of reusable launch vehicles," Contractor Rep. ATR-2007(5309)-1, Aerospace Corporation, CA, 2007.

4. Gilllman, E. D., J. E. Foster, and I. M. Blankson, "Review of leading approaches for mitigating hypersonic vehicle communications blackout and a method of ceramic particulate injection via cathode spot arcs for blackout mitigation," NASA/TM-2010-216220, NASA, Washington, DC, 2010.

5. Morabito, D. D., "The spacecraft communications blackout problem encountered during passage or entry of planetary atmospheres," *IPN Progress Report 42-150*, 1–16, Aug. 2002.

6. Liu, S., Z. Tao, M. Liu, and W. Hong, "WKB and FDTD analysis of Terahertz band electromagnetic characteristics of target coated with unmagnetized plasma," *Journal of Systems Engineering and Electronics*, Vol. 19, No. 1, 1520, 2008.

7. Shi, L., B. Guo, Y. Liu, and J. Li, "Characteristic of plasma sheath channel and its effect on communication," *Progress In Electromagnetic Research*, Vol. 123, 321–336, 2012.

8. Shi, L., B. W. Bai, Y. M. Liu, and X. P. Li, "Navigation antenna performance degradation caused by plasma sheath," *Journal of Electromagnetic Waves and Applications*, Vol. 27, No. 4, 518–528, 2013.

9. Zhao, L., B. W. Bai, W. M. Bao, and X. P. Li, "Effects of reentry plasma sheath on GPS patch antenna polarization property," *International Journal of Antennas and Propagation*, Article ID 823626, 2013.

10. Liu, J. F., X. L. Xi, G. B. Wan, and L. L. Wang, "Simulation of electromagnetic wave propagation through plasma sheath using the moving-window finite-difference time-domain method," *IEEE Transactions on Plasma Science*, Vol. 39, No. 3, 852–855, 2011.

11. Ohler, S. G., B. E. Gilchrist, and A. D. Gallimore, "Electromagnetic signal modification in a localized high-speed plasma flow: Simulations and experimental validation of a stationary plasma thruster," *IEEE Transactions on Plasma Science*, Vol. 27, No. 2, 587–594, 1999.

12. Gao, P., X. P. Li, Y. M. Liu, M. Yang, and J. Li, "Plasma sheath phase fluctuation and its effect on GPS navigation," *2012 10th International Symposium on Antennas, Propagation & EM Theory (ISAPE)*, 579–582, Xi'an, China, 2012.

13. Yang, M., X. P. Li, Y. M. Liu, L. Shi, and X. L. Wang, "Characteristic of time-varying plasma sheath channel," *2012 10th International Symposium on Antennas, Propagation & EM Theory (ISAPE)*, 575–578, Xi'an, China, 2012.

14. Josyula, E. and W. Bailey, "Governing equations for weakly ionized plasma fields of aerospace vehicles," *Journal of Spacecraft and Rockets*, Vol. 40, No. 6, 845–857, 2003.

15. COESA, *U.S. Standard Atmosphere*, U.S. Government Printing Office, Washington, DC, 1976.

16. Kistler, A. L., "Fluctuation measurements in a supersonic turbulent boundary layer," *Physics of Fluids*, Vol. 2, 290–296, May 1959.

17. Fisher, M. C., "Boundary layer surveys on a nozzle wall at $M = 20$ including hot-wire fluctuation measurements," *AIAA 3rd Fluid and Plasma Dynamics Conference*, 1970.

18. Lin, T. C. and L. K. Sproul, "Influence of reentry turbulent plasma fluctuation on EM wave propagation," *Computers & Fluids*, Vol. 35, 703–711, 2006.

19. Demrtriades, A. and R. Grabow, "Mean and fluctuating electron density in equilibrium turbulent boundary layers," *AIAA*, Vol. 9, 1533–1538, 1971.

20. Lederman, A. J. and A. Demetriades, "Mean and fluctuating measurements in the hypersonic boundary layer over a cooled wall," *Journal of Fluid Mechanics*, Vol. 63, 121–144, 1974.

21. Yee, K. S., "Numerical solution of initial boundary value problems involving Maxwell's equation is isotropic media," *IEEE Transactions on Antennas and Propagation*, Vol. 14, 302–307, 1966.

22. Taflove, A. and S. C. Hagness, *Computational Electrodynamics: The Finite-difference Time-domain Method*, 3rd edition, Artech House Publishers, 2005.

23. Dong, X. T., W. Y. Yin, and Y. B. Gan, "Perfectly matched layer implementation using bilinear transform for microwave device applications," *IEEE Transactions on Microwave Theory and Technique*, Vol. 53, No. 10, 3098–3105, Oct. 2005.

24. Wang, H. S. and N. Moyaeri, "Finite-state Markov channel — A useful model for radio communication channels," *IEEE Trans. Veh. Technol.*, Vol. 44, No. 2, 163–171, Feb. 1995.

25. Sadeghi, P., R. A. Kennedy, P. Rapajic, and R. Shams, "Finite-state Markov modeling of fading channels — A survey of principles and applications," *IEEE Signal Process. Mag.*, Vol. 25, No. 5, 57–80, Sep. 2008.

26. Lin, H. P. and M. J. Tseng, "Two-layer multistate Markov model for modelling a 1.8 GHz narrow-band wireless propagation channel gin urban Taipei city," *IEEE Trans. Veh. Technol.,* Vol. 54, No. 4, 435–446, Mar. 2005.

27. Morgadinho, S., R. F. S. Caldeirinha, M. O. Al-Nuaimi, et al., "Time-variant radio channel characterization and modelling of vegetation media at millimeter-wave frequency," *IEEE Transactions on Antennas and Propagation*, Vol. 60, No. 3, 1557–1568, Mar. 2012.